Materials Science & Engineering B 228 (2018) 84–90

Contents lists available at ScienceDirect

Materials Science & Engineering B

journal homepage: www.elsevier.com/locate/mseb

Alloyed monolayers of Cu, Ag, Au and Pt in hexagonal phase: A comprehensive first principles study

Pooja Kapoor[a,*], Arun Kumar[b], Munish Sharma[a], Jagdish Kumar[c], Ashok Kumar[d], P.K. Ahluwalia[a,*]

[a] Department of Physics, Himachal Pradesh University, Shimla, Himachal Pradesh, India
[b] Department of Physics, Swami Vivekananda Govt College, Ghumarwin, Bilaspur, Himachal Pradesh, India
[c] Department of Physics and Astronomical Science, Central University of Himachal Pradesh, Dharamshala, Himachal Pradesh, India
[d] Department of Physical Sciences, School of Basic and Applied Sciences, Central University of Punjab, Bathinda, Punjab, India,

ARTICLE INFO

Keywords:
DFT
Monolayers
Band structure
Mechanical properties
STM images
NDR region

ABSTRACT

We present density functional theory (DFT) based comprehensive study of two-dimensional (2D) alloyed monolayers of noble metals (AgCu, AgPt, AgAu, AuCu, AuPt and CuPt) in hexagonal phase within numerical atomic orbitals and plane wave basis sets methods. The monolayers considered exhibit positive phonon frequencies suggesting them to be dynamically stable. The Pt containing alloyed monolayers have superior structural stability (binding energy and tensile strength) and exhibit metallic and ferromagnetic character amongst all the alloyed monolayers. Interestingly, alloying of Au monolayer with Cu and Ag show semiconducting behavior whereas alloyed AgCu monolayer posseses Dirac-cone like features at high symmetry points. These distinct features in electronic structures of alloyed 2D monolayers have been captured in STM like set up. An anisotropic behavior has been observed in dielectric spectra for all the considered structures. Tunneling characteristics show NDR region for Pt containing alloyed monolayers. The considered alloyed monolayers may potentially be useful as a building blocks for the applications in nano- and opto-electronics.

1. Introduction

Two-dimensional (2D) form of noble-metals with thickness in few nanometer range, possesses unique physical [1] and chemical properties [2]. These have numerous technological applications such as in catalysis, micro electromechanical and nano-electromechanical systems, as interconnects in molecular circuits, sensors, devices for surface enhanced Raman spectroscopy, as protective coatings and biomedical area [3–6]. Noble-metal nanostructures are reported to be synthesized in different polymorphs such as triangular, hexagonal and helical structures as compared to FCC structure in their bulk counterpart [7]. It is known that the properties of metal nanostructures are closely related to their crystal structure [8,9]. Noble metals exhibit various crystal structures in the bulk form, for example, Ag possesses two different polymorphs 9R- [10] and 4H-polytype [11]. The occurrence of hexagonal phase in one-dimensional (1D) hetero-nanostructures [12], thin films [13], nanorods [14–17], and nanowires of Silver has been reported in previous studies [18,19].

A crystallization pathway for metastable HCP phase in gold has recently been reported by Marshall et al. [20]. In last decade it has also been possible to synthesize Gold in various nanostructures such as nanoparticles [21], nanowires [22], nanobelts or nanoribbons [23,24], nanoplates [6] nanosheets [25] and nanotubes [26] with HCP structure. This occurrence of nanostructures of Gold in HCP structure makes understanding of their properties interesting from basic research as well as technological point of view.

Despite wide applications of noble metal nanoplates and nanosheets, their use is limited due to their scarce reserves and high costs. Alloying of noble metals with earth abundant metals has enhanced their properties in a cost effective manner [27]. Alloyed nanomaterials in which d-band vacancies of a Group 8 and 10 (Fe, Pt) metal are progressively filled by a Group 11 (Au, Ag and Cu) metal have attracted wide interest for its application in the field of electronics [28–31]. Note that the heterogeneous Au–Pt [32,33], Au-Ag [34] and Au-Cu [35] nanostructures with much better properties than their pristine counterparts have been synthesized for applications in various fields like optics, electronics, protective coatings, bio-sensing, drug delivery and catalysis [6,30–35].

Though hexagonal structure is not an obvious choice for noble metal alloyed sheets, but motivated by the above mentioned recent reports,

* Corresponding authors.
E-mail addresses: pupooja16@gmail.com (P. Kapoor), pk_ahluwalia7@yahoo.com (P.K. Ahluwalia).

https://doi.org/10.1016/j.mseb.2017.11.011
Received 25 July 2017; Received in revised form 31 October 2017; Accepted 9 November 2017
0921-5107/ © 2017 Elsevier B.V. All rights reserved.

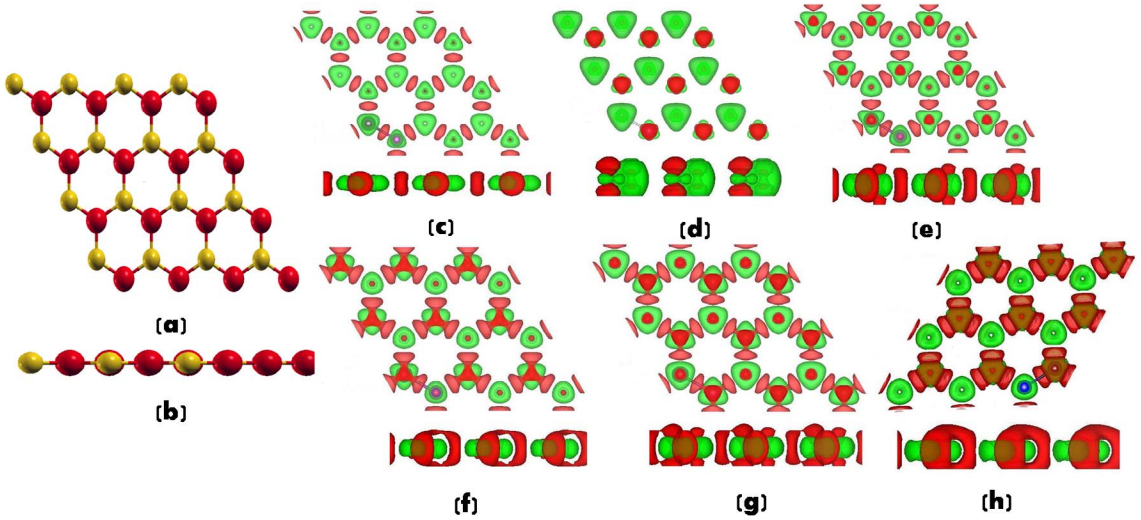

Fig. 1. (a) Top and (b) side view of Crystal structure of one of the studied alloyed monolayers and Top and side view of charge density profiles of all studied systems (c) AgCu, (d) AgPt, (e) CuPt, (f) AuCu, (g) AuPt and (h) AuAg respectively at an isosurface value of 0.004 e/Å^3. Here red/green regions show charge accumulation/depletion. (For interpretation of the references to colour in this figure legend, the reader is referred to the web version of this article.)

and in search of new low cost materials with enhanced properties, we present a DFT-based computational study of alloyed monolayers in hexagonal phase. Our hexagonal monolayers are structurally similar to h-BN monolayer grown on Cu foil [36], where two adjacent edges of h-BN layer are boron terminated and other two are nitrogen terminated. Similarly in our case two adjacent edges are terminated by two different noble-metal, thereby, forming an alloyed noble-metal monolayer (Fig. 1). In order to have faith in our results, we have performed DFT based calculations using two different approaches i.e. localized orbital basis approach as implemented in *SIESTA* (*Spanish Initiative for Electronic Simulation with Thousand of Atoms*) and Plane wave basis approach in *VASP* (Vienna Ab initio Simulation Package). As a result, a comprehensive DFT based comparative study of structural, electronic, magnetic, mechanical and dielectric properties of noble-metal alloyed monolayers is presented. The phonon frequencies at high symmetry points are calculated to check the dynamical stability of the studied systems. To visualize the distinct electronic band structure features of alloyed monolayers, STM analysis is also presented. Here the word *alloy* is being used merely for ease of expression and not be taken in strict sense.

2. Computational details

The computational details for two DFT based first principle approaches, *SIESTA* [37] and *VASP* [38,39] for the study are as follows:

For *SIESTA*, we have used well tested [40,41] Troullier Martin, norm conserving relativistic pseudopotentials [42,43] in fully separable Kleinman and Bylander form. For *VASP*, pseudopotentials used were based on projected augmented wave (PAW) method [44]. The exchange and correlation energies were treated within the generalized gradient approximation (GGA) according to the Perdew-Burke-Ernzerhof (PBE) parameterization for both codes [45]. In *SIESTA*, numerical atomic orbitals (NAOs) with double zeta polarization (DZP) basis set with confinement energy of 30 meV have been used for geometry optimization. Minimization of energy has been carried out using standard conjugate-gradients (CG) technique for both codes until the forces on each atom were less than 0.01 eV/Å. A Monkhorst-Pack [46] of 50 × 50 × 1 k points has been used for sampling the Brillouin zone for both codes. The mesh cutoff energy has been taken equal to 350 Ry in *SIESTA* and corresponding plane wave cutoff energy in *VASP* was taken equal to 400 eV. A unit cell of two atoms, one atom each of the two noble-metals forming the alloy and a vacuum of 16 Å along c axis to avoid interactions between periodic images, were taken for the calculations.

The dielectric properties have been calculated by using first-order time-dependent perturbation theory as implemented in *SIESTA code* [47,48]. A 90 × 90 × 3 optical mesh and 0.04 eV optical broadening are used for optical spectra. It is necessary to include a Drude term associated with intra-band transitions in case of metals, for which the values of τ for all studied systems is taken as 0.001 Ha [40,41]. The dielectric properties in *VASP* were calculated using perturbation theory with local field effects using random phase approximation.

We have also calculated the phonon frequencies using *VASP* code. In addition, tunneling characteristics are calculated within Tersoff and Hamann approximation [49] using STM-like setup. According to this approximation, tunneling current (I) is proportional to the local density of states (LDOS) of the sample. Local Density of states and atomic positions of monolayer samples are obtained from VASP code. For STM analysis, the STM tip was taken of silicon cluster and bias voltage of ± 0.5 V is applied between the STM tip and the sample. STM images are obtained using WsxM software [50] which uses LDOS of *SIESTA* as input.

3. Results and discussion

3.1. Structural properties

Table 1 lists the calculated values of lattice constant, bond length and binding energies of the studied systems. Note that the structural properties of pristine noble metal monolayers are reported in our previous study [40].

The values of lattice constant for these studied alloyed monolayers

Table 1
The comparison of values of lattice constant, bond length and binding energies for alloyed monolayers. The values in bracket are obtained from VASP code.

Property	AgCu	AuCu	AuAg	AuPt	AgPt	CuPt
Lattice constant (Å)	4.34 (4.27)	4.33 (4.21)	4.69 (4.58)	4.47 (4.35)	4.53 (4.41)	4.19 (4.08)
Bond length (Å)	2.53 (2.45)	2.50 (2.42)	2.64 (2.64)	2.55 (2.50)	2.57 (2.54)	2.37 (2.35)
Binding energy (eV)	−2.38 (−2.24)	−2.57 (−2.68)	−2.22 (−2.29)	−3.17 (−3.13)	−2.86 (−2.68)	−3.36 (−3.24)

(Table 1) are lying within the range of their pristine counterparts [40]. The lattice constant varies in the following order AuAg > AgPt > AuPt > AgCu > AuCu > CuPt. The values of bond length (Table 1) are smaller than the average value of their pristine systems (Table S1) which favors the formation of these alloyed monolayers [41]. The value of lattice constant and bond lengths of the studied systems from both SIESTA and VASP calculations are found to be close to each other with a difference (Table 1) of about 2–3%.

The negative value of binding energy (Table 1) in each case suggests that all systems are energetically stable. The value of binding energies of alloyed systems is found to be more than the average value of their (Table S1) pristine counterparts, showing that the alloyed monolayer are more stable than their pristine counterparts and alloy formation is favored. The binding energies follow the trend CuPt > AuPt > AgPt > AuCu > AgCu > AuAg from both SIESTA and VASP calculations. Note that (Table 1) the values obtained from two codes differ by about 6%. It is noted here that amongst the studied alloyed monolayers, the Pt containing systems (e.g. CuPt monolayer) are energetically more stable.

In order to gain an insight into the inter-atomic interactions in noble metal alloyed monolayers, we have calculated the charge density difference profile (Fig. 1). The charge density difference is defined as $\Delta\rho = \rho_{total} - (\rho_{atom1} + \rho_{atom2})$. Charge density difference plot indicates the redistribution of charge between the atoms of different noble-metals. The redistribution is more pronounced for AuCu, CuPt and AuPt as compared to other systems. These results are in agreement with Mulliken charge transfer values given in Table S2 (Supplementary information). These charge transfer mechanisms between the atoms of different species can be explained on the basis of their electronegativities [51]. The higher electronegative atom gains charge while lesser electronegative atom losses charge. From Table S2 it is clear that amongst the chosen systems, AuPt monolayer has the highest charge transfer and AgPt monolayer has the least charge transfer.

3.2. Phonon dispersion spectra for alloyed monolayers

In order to check the dynamical stability of systems considered, we have calculated the phonon frequencies at high symmetry points 'Γ', 'M' and 'K', using VASP code. Two atoms in the unit cell of given systems results in six phonon frequencies, out of which three correspond to acoustic (A) modes and three are optical (O) modes. These modes are associated with out-of-plane (Z), in-plane longitudinal (L), and in-plane transverse (T) symmetries. The lower phonon frequencies correspond to the acoustic mode and higher to the optical mode. The phonon frequencies are given in Table 2 and are found to be positive for all modes at all high symmetry points, which suggests all studied alloyed monolayers to be dynamically stable.

3.3. Mechanical properties

Strain plays an important role when a crystal is compressed or stretched from its equilibrium position. It can affect the device performance and can be applied intentionally to improve device's applications in NEMS (nano electro-mechanical systems) and NOMS (nano opto-mechanical systems). We have applied the biaxial tensile strain which can be modeled by varying the lattice constant in both 'a' and 'b' directions simultaneously, and the corresponding stress tensor values can be obtained. Stress varies directly with strain up to some limit and then decreases [(Fig. 2) for AgCu, AuAg and AuPt systems and Fig. S1 of Supplementary information for AuCu, CuPt and AgPt systems].

The maximum value of strain up to which stress varies directly with strain, gives the value of ultimate tensile strain and corresponding value of stress gives the ultimate tensile strength of the system. The tensile strength of a system is simply the ability of a system to withstand load. The values of ultimate tensile strain and strength for all studied systems as obtained from both codes SIESTA and VASP are given in Table 3 for the comparison.

It is noted that the values of tensile strength of alloyed monolayer lies within the range of its pristine counterparts [40]. In case of Pt containing systems, the tensile strength is less than pristine Pt monolayer and more than other constituent atom of alloyed monolayer. Amongst the studied systems, CuPt has the highest tensile strength that varies as CuPt > AuPt > AuCu > AgPt > AgCu > AuAg. This trends is attributed to the stronger bonding as reflected by binding energies of the studied systems.

3.4. Electronic and magnetic properties

To understand the electronic properties of alloyed monolayers, electronic band structure and corresponding spin polarized total and partial density of states as a function of energy have been plotted and are shown in Fig. 3 for AgCu, AuAg, AuCu and CuPt monolayer and Fig. S2 (Supplementary information) for AuPt and CuPt monolayer. The band structures obtained from SIESTA and VASP calculations are found to be similar [(Fig. S3) of Supplementary information]. The electronic band structures for various systems under study have been calculated along the Γ-M-K-Γ direction of the Brillouin zone. From the electronic band structure, it is observed that all Pt containing alloyed monolayers (AuPt, AgPt and CuPt) are metallic in nature and their features are quite similar to the electronic band structure of pristine Pt monolayer reported in previous study [40].

The Au containing alloyed monolayers (AuCu and AuAg) are semiconducting in nature. An indirect band gap of 0.46 eV is calculated for AuCu monolayer which lies between M and K high symmetry point of Brillouin zone. AuAg monolayer, shows a direct band gap of 0.88 eV at M high symmetry point. The values of band-gaps from VASP and SIESTA calculations differ by a small amount of less than 2% [(Table S3) of Supplementary information]. A similar behavior is also observed for the alloyed nanowires of these noble metals in previous studies [41]. In AgCu monolayer, two conical intersections (Dirac-cone like behavior) crossing the Fermi-level, one from the conduction band at high symmetry point M and other from the valence band at high symmetry point K are observed. AgCu monolayer shows similar behavior as seen in band structures of pristine Ag and Cu monolayers [40].

In order to have a deeper insight into the contribution of different orbitals of an atom in the band formation, we have analyzed the partial

Table 2
The value of phonon frequencies at Γ, M and K high symmetry points for all studied alloyed monolayers.

System	Phonon Frequencies (in cm^{-1})		
	at Γ	at M	at K
AgCu	219.576, 219.07, 52.675, 7.85, 1.02, 0.87	217.465, 167.32, 117.675, 63.94, 6.32, 2.836	182.49, 180.764, 158.067, 9.888, 4.944, 4.065
AgPt	172.16, 166.48, 75.95, 8.466, 0.494, 0.0054	229.123, 223.125, 94.193, 16.022, 8.271, 0.025	150.14, 109.32, 87.167, 8.964, 0.594, 0.35
CuPt	174.136, 148.75, 28.304, 9.85, 1.86, 0.606	257.464, 109.97, 108.61, 106.85, 10.315, 4.356	217.84, 93.47, 19.58, 18.71, 5.54, 5.20
AuPt	108.63, 92.403, 88.15, 10.52, 2.96, 0.446	283.88, 213.594, 87.267, 51.77, 27.145, 0.0425	270.063, 265.207, 153.60, 6.07, 3.87, 3.157
AuCu	239.25, 238.84, 50.661, 24.167, 1.0012, 0.901	242.41, 222.766, 115.97, 50.12, 11.22, 0.1515	166.50, 89.08, 85.214, 17.027, 10.204, 8.337
AuAg	164.03, 164.0, 55.43, 9.164, 0.172, 0.099,	84.64, 83.75, 113.704, 9.664, 2.19, 1.702	176.044, 116.493, 84.3, 11.34, 9.20, 0.512,

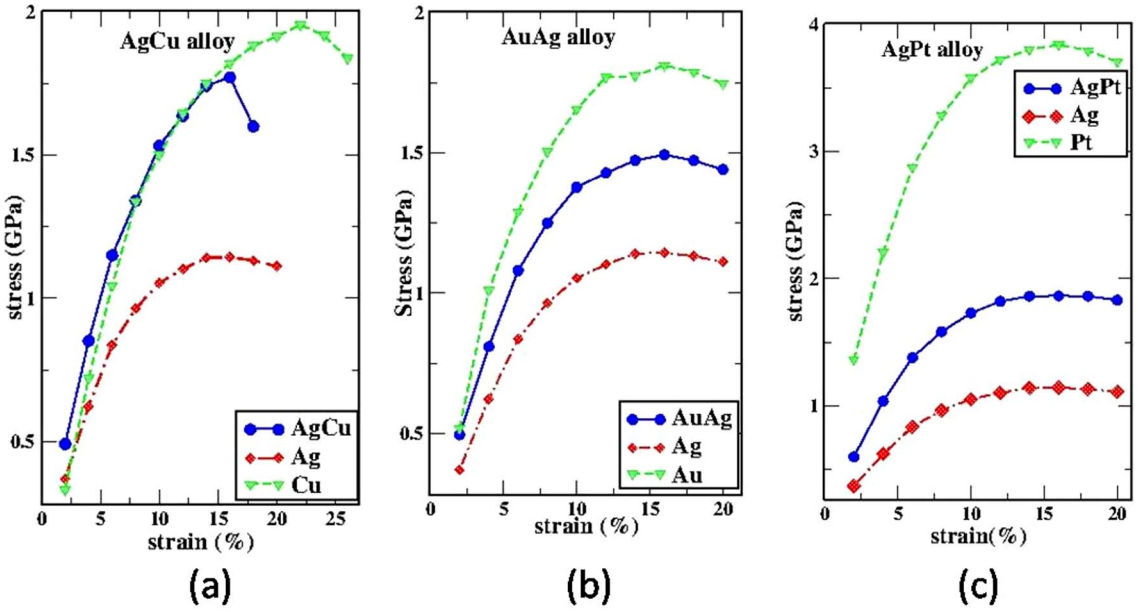

Fig. 2. Stress-strain curves to determine the ultimate tensile strength for the alloyed monolayers (a) AgCu, (b) AuAg and (c) AgPt respectively where strain is in (%) and stress is in (GPa).

Table 3
The values of magnetic moment (μ_b), tensile strength, and tensile strain in case alloyed monolayers. The values given in bracket are the values obtained from VASP calculations for comparison.

Property	AgCu	AuCu	AuAg	AuPt	AgPt	CuPt
Magnetic moment (μ_b)	0.00 (0.0)	0.00 (0.0)	0.00 (0.0)	0.58 (0.57)	0.41 (0.36)	0.45 (0.51)
Tensile strength (GPa)	1.77 (1.46)	1.97 (2.32)	1.49 (1.35)	2.49 (2.52)	1.86 (1.81)	2.64 (2.62)
Tensile strain (%)	16 (14)	16 (14)	16 (14)	14 (14)	16 (14)	20 (14)

density of state plots (Figs. 3 and S2) of the studied systems. In the density of states plots of all Pt containing alloyed monolayers (AuPt, AgPt and CuPt), a major contribution to the density of states is due to Pt 5d orbitals near the Fermi-level. In case of Cu containing alloyed monolayers (AuCu and AgCu), Cu 3d orbitals show a major contribution to the density of states at the Fermi-level. In AuAg system, 5d orbitals of Au give a major contribution to the density of states near the Fermi-level.

The quantum ballistic conductance of a system under ideal situation can be determined by the number of bands crossing the Fermi-level (E_f) [52]. For each band crossing the Fermi-level (E_f), the ballistic conductance is G_0 which results into a conductance of nG_0 for n number of bands crossing the Fermi-level. The calculated quantum ballistic conductance is $4G_0$ for AgPt, CuPt and AgCu systems while $6G_0$ for AuPt monolayer. The conductance is zero for AuAg and AuCu as these systems are found to be semiconducting in nature with no band crossing the Fermi-level.

The alloyed monolayers containing Pt (AgPt, AuPt and CuPt) are found to be magnetic in nature as is clear from their density of states plots [(Fig. 3(d)) for CuPt and Fig. S2 of Supplementary information for AuPt and AgPt]. The spin up and spin down states are different in magnitude, with spin up states showing a major contribution, that favors ferromagnetism. The major contribution to ferromagnetism comes from the d-orbitals and particularly from the Pt 5d orbitals. All other studied systems are non-magnetic, with both spin up and spin down density of states having equal magnitude resulting in no net magnetic moment. The **Stoner criterion** is a condition to be fulfilled for the ferromagnetic order to arise in a solid. According to Stoner criterion, ferromagnetism can arise in a system if:

$$I \times N_{E_f} \geqslant 1$$

which is getting fulfilled for our Pt containing systems. Here I is the stoner parameter whose value is 0.63 eV for Pt [53] and N_{E_f} is the non-magnetic density of states of major contributing orbital (Pt 5d orbitals here) at the Fermi-level. The values of Stoner criterion (IN_{E_f}) are given in Table S4.

We have also calculated the magnetic moment as given in Table 3 ($(\mu_b = Q_\uparrow - Q_\downarrow)$, where $Q_\uparrow$ in the Mulliken charge population for the spin up and $Q_\downarrow$ is the Mulliken charge population for the spin down states) showing clearly the presence of ferromagnetism. The magnetic moments have also been calculated with VASP code and show a similar trend with a difference of about 2% in case of AuPt and 12% in case of AgPt and CuPt.

3.5. STM analysis

The distinct features in electronic band structure of alloyed monolayers (i.e. semi-conducting or metallic behavior) offer a suitable platform for the simulated STM calculations. STM topographical images are an important tool for providing significant structural and electronic information. The distinct electronic band structure features (semi-conducting or metallic) are clearly visible in their STM images (Fig. 4) and may act as electronic fingerprints for comparison with experimental STM. The difference in the brightness of STM images is directly proportional to the magnitude of tunneling current passing through the sample when forward biased. The semi-conducting alloyed monolayers show faded spots showing very small tunneling current which is due to absence of channels near Fermi-level. The STM images for Pt containing alloyed monolayers have very bright spots showing larger magnitude of tunneling current which is due to presence of available channels near Fermi-level.

The tunneling characteristics are given in Fig. S4 (Supplementary information) and are in good agreement with obtained STM images of studied systems. These characteristics clearly show distinct features for semiconducting (AuCu and AuAg) and metallic (AgCu, CuPt, AgPt and AuPt) systems. The magnitude of current is low for semiconducting systems and high for metallic systems. In case of semiconducting systems, tunneling current is zero within the band gap range while the metallic systems (CuPt, AgPt and AuPt) show negative differential

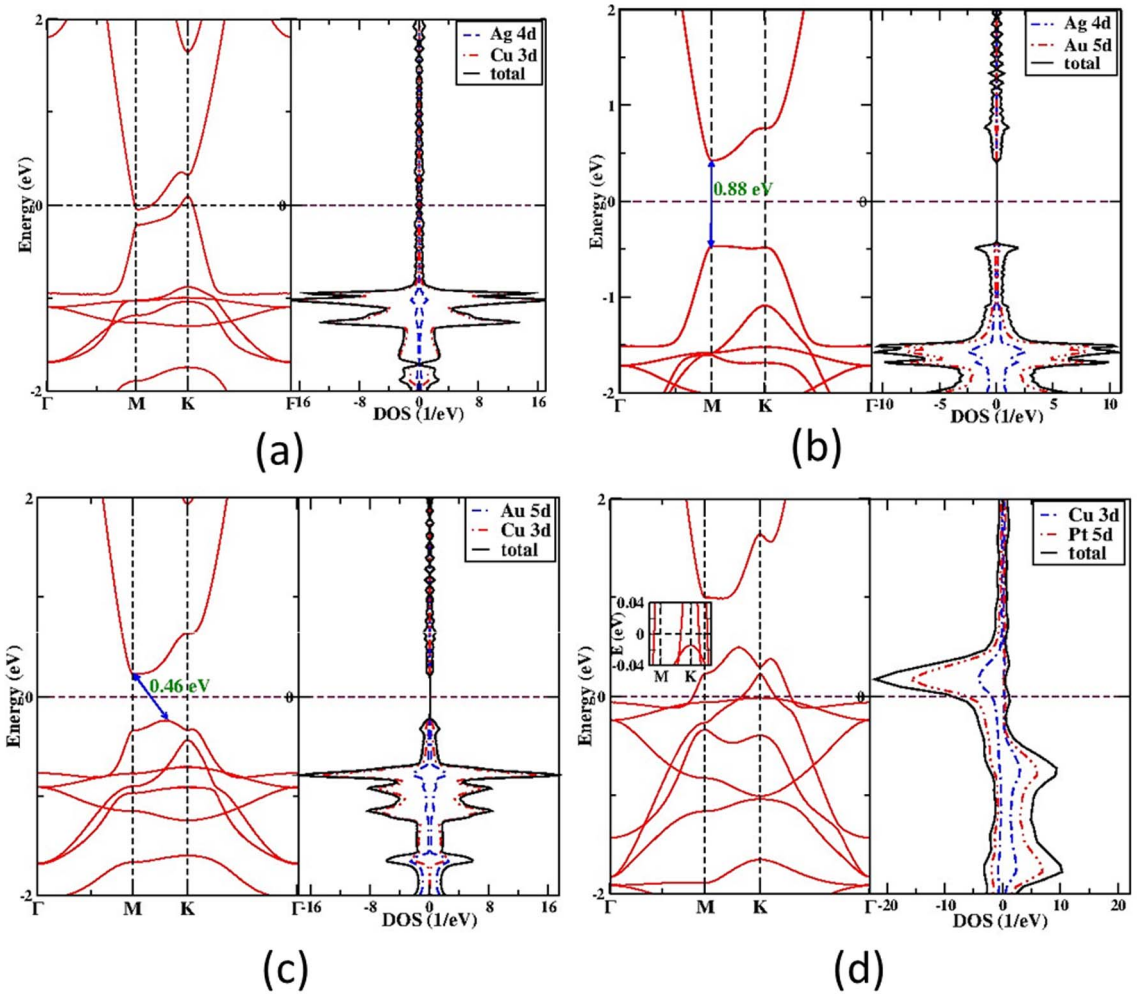

Fig. 3. Electronic band structure and density of state for the alloyed monolayers (a) AgCu, (b) AuAg and (c) AuCu and CuPt respectively. The Fermi-level is set at 0 eV. The values of band-gap for AuAg have been given in figure and the number of bands crossing the Fermi-level in CuPt has been shown in inset. The contribution from s orbitals in the density of states was very less, so they have not been shown here.

resistance (NDR). NDR is a unique property occurring rarely in some electronic circuits and devices where a decrease in current is observed with increase in voltage across the terminal, resulting in negative resistance [54,55]. NDR is of great significance in device applications such as electronic oscillators, amplifiers, switching and memory devices [56,57].

3.6. Dielectric properties

Furthermore, real and imaginary parts of dielectric function ε_1 and ε_2, electron energy loss spectra (EELS), reflectance and absorption spectra for the systems under study have been shown in Figs. 5 and S5 of Supplementary information. The real and imaginary part of dielectric function as obtained from SIESTA and VASP calculation are plotted together in Fig. S6 and trends are found to be similar. When ε_1

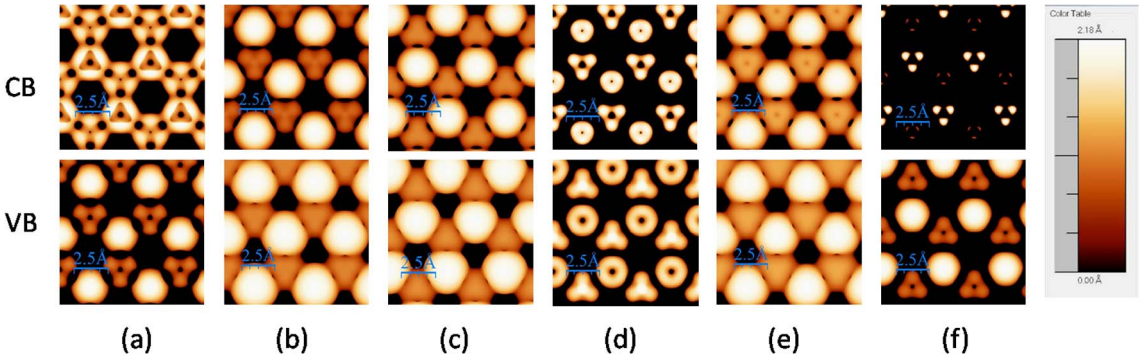

Fig. 4. Simulated STM topographical images of a 11 Å × 11 Å area of (a) AgCu, (b) AgPt, (c) CuPt, (d) AuCu, (e) AuPt and (f) AuAg alloyed monolayers respectively at ± 0.5 V bias voltage and an isosurface value of 0.00125 eV/Å^3 where dark black areas show absence of tunneling current due to filled orbitals and bright spots indicate presence of tunneling current due to unfilled orbitals.

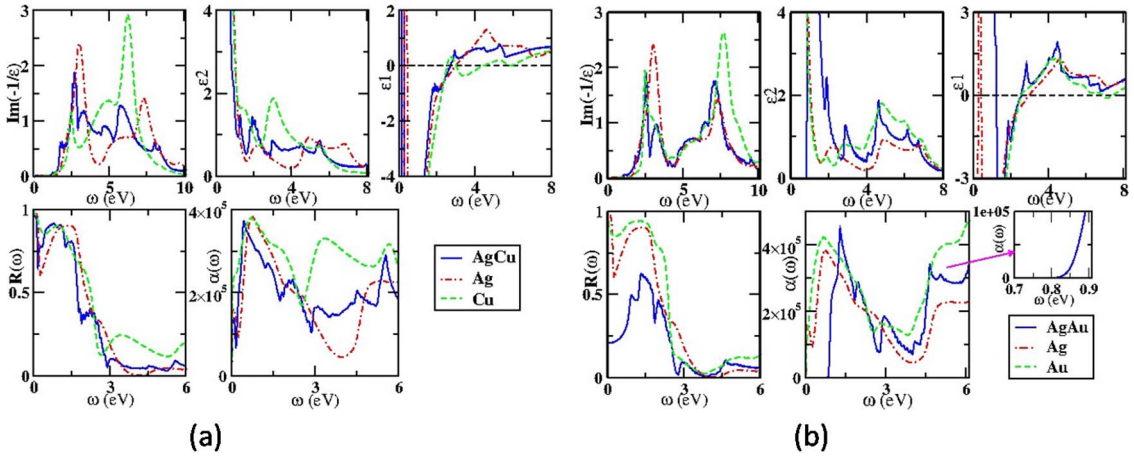

Fig. 5. The figure shows the plots of real (ε_1) and imaginary parts (ε_2) of dielectric function (ε), EELS spectra, absorption spectra (α) and the reflectance spectra (R) for alloyed monolayers (a) AgCu and (b) AuAg respectively and its comparison with their pristine counterparts. The rising edge of absorption peak for AuAg is shown in the inset.

approaches zero, we observe a sharp resonance peak in EELS, which gives the value of plasmon frequency (ω_p). The structural peaks associated with ε_2 are on account of inter-band transitions across E_f in the corresponding electronic band structure. From the Table S5, it was found that the structural peaks in ε_2 for alloyed monolayers systems are generally found to lie in between the values of pristine monolayers [40].

EELS show sharp resonance peaks giving the value of plasmon frequency (ω_p) for the various systems under study (Table S5). These peaks represent the collective excitation of electrons (plasmons) at these energies. From Table S5 it follows that value of plasmon frequencies of alloyed monolayers are similar to the values of pristine monolayers and lies in between the values for pristine counterparts [40]. It is found that reflectance spectra for metallic systems shows sharp dip that corresponds to the collective excitation of electrons and this sudden change reveals reflectance edge. The reflectance edge for the studied metallic alloyed monolayers (except AgCu) lies in infrared region (0 eV–1.65 eV) while for AgCu it lies in visible region (1.65 eV–3.2 eV) (Table S5). Hence, they are found to be transparent to the visible radiations.

Note that AuCu and AuAg monolayers show semiconducting nature, and hence have no reflecting properties, so we study absorption spectra in their case. The AuCu and AuAg monolayers have band gap in IR region and hence will absorb the radiations higher than their corresponding band gaps and appear blackish. The rising edge in the absorption spectra indicates that the systems absorb the radiations higher than their band gaps. The corresponding values of the absorption edge are similar to their band gaps as given in Table S5 (Supplementary information).

4. Conclusions

In summary, a comparative density functional theory (DFT) based comprehensive study has been reported to investigate structural, electronic, magnetic, mechanical, dielectric, vibrational and transport properties of ultrathin alloyed nanostructures (AuCu, AuAg, AuPt, AgCu, AgPt and CuPt) in hexagonal structure.

- The lattice constant values for alloyed monolayers lie close to their pristine counterparts.
- The value of binding energy for these alloyed structures is more than the average binding energy of their pristine counterparts showing the alloyed structure to be energetically more stable.
- Pt-containing alloyed monolayers posses higher binding energy.
- The phonon frequencies for all studied alloyed monolayers are positive for all modes at all high-symmetry points suggesting the systems to be dynamically stable.
- The Pt-containing alloyed monolayers are metallic and ferromagnetic in nature with higher tensile strengths.
- The Au containing alloyed monolayers (AuCu and AuAg) are semiconducting with a band-gap of about 0.46 eV and 0.88 eV, respectively.
- The reflectance edge and absorption edge for the alloyed monolayers lies in the infrared region.
- The distinct features in electronic band structures of alloyed monolayers are clearly visible in their tunneling characteristics and STM images.
- The considered alloyed monolayers may be useful for the applications in nanoelectronic, optoelectronic, magnetoelectronics and spintronics.

Acknowledgements

Pooja Kapoor wishes to acknowledge the financial support from University Grants Commission (UGC), New Delhi in the form of University Grants Commission Basic Sciences Research (UGC-BSR) Senior Research Fellowship (SRF). All the calculations have been carried on High Performance Computing Cluster (HPCC) in Physics Department at H.P. University, provided by Department of Science & Technology, Government of India under Funds for the Improvement of Science & Technology (FIST) programme. This research did not receive any specific grant from funding agencies in the public, commercial, or not-for-profit sectors.

Appendix A. Supplementary data

Supplementary data associated with this article can be found, in the online version, at http://dx.doi.org/10.1016/j.mseb.2017.11.011.

References

[1] A.K. Geim, K.S. Novoselov, The rise of graphene, Nat. Mater. 6 (2007) 183–191.
[2] F. Geng, R. Ma, A. Nakamura, K. Akatsuka, Y. Ebina, Y. Yamauchi, N. Miyamoto, Y. Tateyama, T. Sasaki, Unusually stable ~100-fold reversible and instantaneous swelling of inorganic layered materials, Nat. Commun. 4 (2013) 1632–1638.
[3] C.C. Li, W.P. Cai, B.Q. Cao, F.Q. Sun, Y. Li, C.X. Kan, L.D. Zhang, Mass synthesis of large single-crystal Au nanosheets based on a polyol process, Adv. Funct. Mater. 16 (1) (2006) 83–90.
[4] N. Krasteva, I. Besnard, B. Guse, R.E. Bauer, K. Mullen, A. Yasuda, T. Vossmeyer, Self-assembled gold nanoparticle/dendrimer composite films for vapor sensing applications, Nano Lett. 2 (5) (2002) 551–555.
[5] S.-J. Hsu, I.J.B. Lin, Synthesis of gold nanosheets through thermolysis of mixtures of long chain 1-alkylimidazole and hydrogen tetrachloroaurate(III), J. Chin. Chem. Soc. 56 (1) (2009) 98–106.
[6] S. Rodriguez-Barrero, J. Fernandez-Larrinoa, I. Azkona, L.N. Lopez de Lacalle, R. Polvorosa, Enhanced performance of nanostructured coatings for drilling by

droplet elimination, Mater. Manuf. Process. 31 (2016) 593–602.
[7] X. Hong, C. Tan, J. Chen, Z. Xu, H. Zhang, Synthesis, properties and applications of one- and two-dimensional gold nanostructures, Nano Res. 8 (1) (2015) 40–55.
[8] J. Kim, Y. Lee, S. Sun, Structurally ordered FePt nanoparticles and their enhanced catalysis for oxygen reduction reaction, J. Am. Chem. Soc. 132 (14) (2010) 4996–4997.
[9] K. Kusada, et al., Discovery of face-centered-cubic ruthenium nanoparticles: facile size-controlled synthesis using the chemical reduction method, J. Am. Chem. Soc. 135 (15) (2013) 5493–5496.
[10] F. Ernst, M.W. Finnis, D. Hofmann, T. Muschik, U. Schönberger, U. Wolf, M. Methfessel, Theoretical prediction and direct observation of the 9R structure in Ag, Phys. Rev. Lett. 69 (4) (1992) 620–623.
[11] D. Novgorodova, A.I. Gorshkov, A.V. Mokhov, Native silver and its new structural modifications, Zap. Vses. Mineral. Obshch. 108 (1979) 552–563.
[12] X.S. Shen, G.Z. Wang, X. Hong, X. Xie, W. Zhu, D.P. Li, Anisotropic growth of one-dimensional silver rod–needle and plate–belt heteronanostructures induced by twins and hcp phase, J. Am. Chem. Soc. 131 (31) (2009) 10812–10813.
[13] P. Taneja, R. Banerjee, P. Ayyub, R. Chandra, G.K. Dey, Observation of a hexagonal (4H) phase in nanocrystalline silver, Phys. Rev. B 64 (3) (2001) 033405.
[14] X.H. Liu, J. Luo, J. Zhu, Size effect on the crystal structure of silver nanowires, Nano Lett. 6 (3) (2006) 408–412.
[15] A. Singh, A. Ghosh, Stabilizing high-energy crystal structure in silver nanowires with underpotential electrochemistry, J. Phys. Chem. C 112 (10) (2008) 3460–3463.
[16] B. Wang, G.T. Fei, Y. Zhou, B. Wu, X. Zhu, L. Zhang, Controlled growth and phase transition of silver nanowires with dense lengthwise twins and stacking faults, Cryst. Growth Des. 28 (8) (2008) 3073–3076.
[17] C. Liang, K. Terabe, T. Hasegawa, M. Aono, Formation of metastable silver nanowires of hexagonal structure and their structural transformation under electron beam irradiation, Japn. J. Appl. Phys. 45 (7) (2006) 6046.
[18] I. Chakraborty, D. Carvalho, S.N. Shirodkar, S. Lahiri, S. Bhattacharyya, R. Banerjee, U. Waghmare, P. Ayyub, Novel hexagonal polytypes of silver: growth, characterization and first-principles calculations, J. Phys.: Condens. Matter 23 (2011) 1–12 325401.
[19] I. Chakraborty, S.N. Shirodkar, S. Gohil, U.V. Waghmare, P. Ayyub, A stable, quasi-2D modification of silver: optical, electronic, vibrational and mechanical properties, and first principles calculations, J. Phys.: Condens. Matter 26 (2014) 1–10 025402.
[20] A.F. Marshall, S.V. Thombare, P.C. McIntyre, Crystallization pathway for metastable hexagonal close-packed gold in germanium nanowire catalysts, Cryst. Growth Des. 15 (2015) 3734–3739.
[21] A.F. Marshall, I.A. Goldthorpe, H. Adhikari, M. Koto, Y.-C. Wang, L. Fu, E. Olsson, P.C. McIntyre, Hexagonal close-packed structure of au nanocatalysts solidified after Ge nanowire vapor–liquid–solid growth, Nano Lett. 10 (9) (2010) 3302–3306.
[22] X. Huang, S. Li, S. Wu, Y. Huang, F. Boey, C.L. Gan, H. Zhang, Graphene oxide-templated synthesis of ultrathin or tadpole-shaped au nanowires with alternating hcp and fcc domains, Adv. Mater. 24 (2012) 979–983.
[23] C.M. Payne, D.E. Tsentalovich, D.N. Benoit, W. Guo, L.J.E. Anderson, V.L. Colvin, M. Pasquali, J.H. Hafner, Synthesis and crystal structure of gold nanobelts, Chem. Mater. 26 (6) (2014) 1999–2004.
[24] Z. Fan, M. Bosman, X. Huang, D. Huang, Y. Yu, K.P. Ong, Y.A. Akimov, L. Wu, B. Li, J. Wu, Y. Huang, Q. Liu, C.E. Png, C.L. Gan, P. Yang, H. Zhang, Stabilization of 4H hexagonal phase in gold nanoribbons, Nat. Commun. 6 (2015) 7684.
[25] X. Huang, S. Li, Y. Huang, S. Wu, X. Zhuo, S. Li, C.L. Gan, F. Boey, C.A. Mirkin, H. Zhang, Synthesis of hexagonal close-packed gold nanostructures, Nat. Commun. 2 (2011) 292.
[26] Y. Oshima, A. Onga, K. Takayanagi, Helical gold nanotube synthesized at 150 K, Phys, Rev. Lett. 91 (20) (2003) 205503-1-205503-4.
[27] J. Wu, P. Li, Y.-T. Pan, S. Warren, X. Yin, H. Yang, Surface lattice-engineered bimetallic nanoparticles and their catalytic properties, Chem. Soc. Rev. 41 (2012) 8066–8074.
[28] X. Teng, M. Feygenson, Q. Wang, J. He, W. Du, A.I. Frenkel, W. Han, M. Aronson, Electronic and magnetic properties of ultrathin Au/Pt nanowires, Nano Lett. 9 (9) (2009) 3177–3184.
[29] M.F. Luo, C.C. Wang, G.R. Hu, W.R. Lin, C.Y. Ho, Y.C. Lin, Y.J. Hsu, Active alloying of Au with Pt in nanoclusters supported on a thin film of Al_2O_3/NiAl(1 0 0), J. Phys. Chem. C 113 (2009) 21054–21062.
[30] G. Selvarani, S.V. Selvaganesh, S. Krishnamurthy, G.V.M. Kiruthika, P. Sridhar, S. Pitchumani, A.K. Shukla, A methanol-tolerant carbon-supported Pt–Au alloy cathode catalyst for direct methanol fuel cells and its evaluation by DFT, J. Phys. Chem. C 113 (17) (2009) 7461–7468.
[31] R.M. Ormerod, C.J. Baddeley, R.M. Lambert, Active alloying of Au with Pt in nanoclusters supported on a thin film of Al_2O_3/NiAl(1 0 0), Surf. Sci. 259 (1–2) (1991) 709–713.
[32] J.B. Jia, L.Y. Cao, Z.H. Wang, Platinum-coated gold nanoporous film surface: electrodeposition and enhanced electrocatalytic activity for methanol oxidation, Langmuir 24 (11) (2008) 5932–5936.
[33] P. Hernandez-Fernandez, S. Rojas, P. Ocon, J.L. Gomez de la Fuente, J. San Fabian, J. Sanza, M.A. Peña, F.J. García-García, P. Terreros, J.L.G. Fierro, Influence of the preparation route of bimetallic Pt–Au nanoparticle electrocatalysts for the oxygen reduction reaction, J. Phys. Chem. C 111 (7) (2007) 2913–2923.
[34] X. Ye, H. Shi, X. He, Y. Yu, D. He, J. Tang, Y. Lei, K. Wang, Cu–Au alloy nanostructures coated with aptamers: a simple, stable and highly effective platform for *in vivo* cancer theranostics, Nanoscale 8 (2016) 2260–2267.
[35] D.X. Li, C.F. Li, A.H. Wang, Q. He, J.B. Li, Hierarchical gold/copolymer nanostructures as hydrophobic nanotanks for drug encapsulation, J. Mater. Chem. 20 (2010) 7782–7787.
[36] K.K. Kim, A. Hsu, X. Jia, S.M. Kim, Y. Shi, M. Hofmann, D. Nezich, J.F. Rodriguez-Nieva, M. Dresselhaus, T. Palacios, J. Kong, Synthesis of monolayer hexagonal boron nitride on Cu foil using chemical vapor deposition, Nano Lett. 12 (2012) 161–166.
[37] J.M. Soler, E. Artacho, J.D. Gale, A. Garcia, J. Junquera, P. Ordejon, D.S. Portal, The SIESTA method for ab initio order-N materials simulation, J. Phys. Condens. Matter. 14 (2002) 2745–2779.
[38] G. Kresse, J. Hafner, Ab initio molecular dynamics for liquid metals, Phys. Rev. B 47 (1) (1993) 558–561.
[39] G. Kresse, J. Furthmuller, Efficient iterative schemes for ab initio total-energy calculations using a plane-wave basis set, Phys. Rev. B 54 (16) (1996) 11169–11186.
[40] P. Kapoor, J. Kumar, A. Kumar, A. Kumar, P.K. Ahluwalia, Electronic mechanical, and dielectric properties of two-dimensional atomic layers of noble metals, J. Electron. Mater. 46 (1) (2017) 650–659.
[41] A. Kumar, A. Kumar, P.K. Ahluwalia, Topology dependent electronic and dielectric properties of free standing alloyed ultrathin nanowires of noble metals, Physica E 62 (2014) 136–146.
[42] N. Troullier, J.L. Martins, Efficient pseudopotentials for plane-wave calculations, Phys. Rev. B 43 (3) (1991) 1993–2006.
[43] N. Troullier, J.L. Martins, Efficient pseudopotentials for plane-wave calculations. II. Operators for fast iterative diagonalization, Phys. Rev. B 43 (1991) 8861–8869.
[44] G. Kresse, D. Joubert, From ultrasoft pseudopotentials to the projector augmented-wave method, Phys. Rev. B 59 (3) (1999) 1758–1775.
[45] J.P. Perdew, K. Burke, M. Ernzerhof, Generalized gradient approximation made simple, Phys. Rev. Lett. 77 (18) (1996) 3865–3868.
[46] J. Moreno, J.M. Soler, Optimal meshes for integrals in real- and reciprocal-space unit cells, Phys. Rev. B 45 (24) (1992) 13891–13898.
[47] F. Knider, J. Hugel, A.V. Postnikov, Ab initio calculation of dc resistivity in liquid Al, Na and Pb, J. Phys. Condens. Matter 19 (2007) 196105.
[48] E.G. Maksimov, I.I. Mazin, S.N. Rashkeev, Yu.A. Uspenski, First-principles calculations of the optical properties of metals, J. Phys. F: Met. Phys. 18 (1988) 833–849.
[49] J. Tersoff, D.R. Hamann, Theory of the scanning tunneling microscope, Phys. Rev. B 31 (2) (1985) 805–813.
[50] I. Horcas, R. Fernandez, J.M. Gomez-Rodriguez, J. Colchero, J. Gomez-Herrero, A.M. Baro, WSXM: A software for scanning probe microscopy and a tool for nanotechnology, Rev. Sci. Instrum. 78 (2007) 013705.
[51] S.K. Chandel, A. Kumar, P.K. Ahluwalia, R. Sharma, A first principle study of encapsulated and functionalized silicon nanotube of chirality (6,6) with monoatomically thin metal wires of Ag Au and Cu, Physica E 68 (2015) 1–7.
[52] B.K. Agrawal, V. Singh, R. Srivastava, S. Agrawal, Ab initio study of the structural, electronic, and optical properties of ultrathin lead nanowires, Phys. Rev. B 74 (2006) 1–12 245405.
[53] O. Gunnarsson, Band model for magnetism of transition metals in the spin-density-functional formalism, J. Phys. F: Met. Phys. 6 (4) (1976) 587–606.
[54] Rudolf F. Graf, Modern Dictionary of Electronics, seventh ed., Newnes, 1999, p. 499 ISBN 0750698667.
[55] A. Kumar, P.K. Ahluwalia, Transport properties of pristine and alloyed free standing ultrathin nanowires of noble metals, J. Alloys Compd. 615 (2014) 194–203.
[56] Mohsen Shahinpoor, Hans-Jörg Schneider, Intelligent Materials, Royal Society of Chemistry, London, 2008, p. 209 ISBN 0854043357.
[57] H. Beneking, ISBN 0412562200, High Speed Semiconductor Devices: Circuit Aspects and Fundamental Behaviour, Springer, 1994, pp. 114–117.

View publication stats